Science Press

ARTICLE

Effect of Repair Welding on Corrosion Behavior of 7N01 Aluminum Alloy Welded Joint

Li Shuai[1,2],   Liu Zhongying[1],   Wang Xingxing[1],   Mao Feng[2],   Xia Yueqing[1],   Jiu Yongtao[3],   Shangguan Linjian[1],   Long Weimin[3]

[1] School of Mechanical Engineering, North China University of Water Resources and Electric Power, Zhengzhou 450045, China; [2] National Joint Engineering Research Center for Abrasion Control and Molding of Metal Materials, Henan University of Science and Technology, Luoyang 471003, China; [3] State Key Laboratory of Advanced Brazing Filler Metals and Technology, Zhengzhou Research Institute of Mechanical Engineering, Zhengzhou 450001, China

Abstract: Mandatory repair welding for production of structural parts easily causes problems to the reliability of welded joints due to the resultant extra thermal cycle. The evolution of corrosion resistance of repair welded joint of 7N01 aluminum alloy in T5 and T4 state through metal inert gas (MIG) welding process was investigated. The results reveal that repair welding deteriorates the corrosion resistance of weldment, especially of the heat-affected zone. The main reason for the change in corrosion resistance of repair weldment is related to the transformation of precipitates and the diffusion of Zn from the matrix to grain boundaries caused by the extra thermal cycles.

Key words: MIG welding; repair welding; 7N01 aluminum alloy; corrosion behavior; heat-affected zone; thermal cycles

---

7N01 aluminum alloys have medium-strength and are widely applied in rail transit because of their high specific strength and good weldability[1-3]. And the metal inert gas (MIG) welding method is commonly applied in assembly of aluminum alloy structures, which is attributed to the advantages of relatively easy operation and low cost[4-8]. Since the 7N01 aluminum alloys are age-strengthened alloys, the corrosion resistance and mechanical strength are mainly related to the thermal cycles[9-11]. Repair welding is often mandatory in actual production of welded structural parts in order to prolong their service lives[12,13]. However, the extra thermal cycles easily cause new problems to the reliability of welded joints. Maya-Johnson et al[12] found that the increase of the number of repair welding decreases the ultimate tensile strength of AA7020 aluminum alloy welded joints. Venugopal et al[13] discussed the effect of repair

welding on the performance of AA2219 aluminum alloy welded joints by tungsten inert gas welding, and then pointed out that the repair welding process exacerbates the solute segregation along the partially melted zone, resulting in the decrease of hardness in this location.

It is frequently necessary to join different types of aluminum alloys to fulfill the requirements of special properties. However, the aluminum alloys have different response mechanisms to welding thermal cycles due to the differences in strengthening mechanism and the initial aging conditions, and usually the heat-affected zones (HAZs) of welded joint soften in different degrees[14,15]. At present, the research on 7N01 aluminum alloy welded joint mainly focuses on the change of microstructure and mechanical properties. However, the effect of repair welding on the corrosion behavior of 7N01 aluminum alloy welded joint is

---

rarely investigated[12,14]. This work aims to illuminate the influence of repair welding on the corrosion susceptibility of the 7N01 aluminum alloy welded joints.
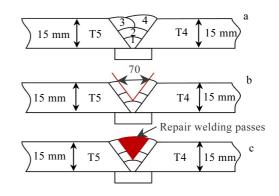
1 Experiment

The 7N01 aluminum alloy in T5 state, namely 7N01-T5, and 7N01 aluminum alloy in T4 state, namely 7N01-T4, were butt welded by MIG welding process with ER5356 filler metal. The chemical composition of the base aluminum alloys and filler wire is listed in Table 1. T5 state means that the aluminum alloy is cooled rapidly after high temperature molding process and then artificially aged. T4 state means that the aluminum alloys are subjected to solution heat treatment and then naturally aged. Fig.1 displays the schematic diagram of repair welding and the corresponding welding parameters are displayed in Table 2. The high-purity argon gas (99.999%) was used as the shield gas. The acronyms were self-defined to stand for different locations in welded joint in this research, as shown in Fig.2 and Table 3.
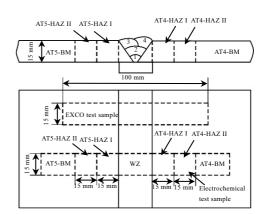
The morphology of the samples after immersion experiment was investigated with scanning electron microscope (SEM). The evolution of precipitates in welded joints was examined by FEI Tecnai G220 transmission electron microscope (TEM) with the operating voltage of 200 kV. TEM samples were thinned to around 30 μm in thickness by mechanical polishing and then electrochemically thinned utilizing a twin jet polisher with 30vol% nitric acid-methyl alcohol solution under the temperature of −30 °C.

The dimensions of exfoliation corrosion (EXCO) specimens and sampling locations are displayed in Fig.2. The specimens were cleaned by acetone to remove contaminants before immersion corrosion tests. The exfoliation corrosion experiment was performed in the corrosion solution of 4.0 mol/L NaCl+0.5 mol/L KNO_3+0.1 mol/L HNO_3 at the constant temperature of 35±2 °C, according to the criterion of GB/T 22639-2008[16]. The intergranular corrosion (IGC)

experiment was carried out in the solution of 1.0 mol/L NaCl+0.01 mol/L H_2O_2 at the constant temperature of 25±2 °C according to the criterion of GB/T 7998-2005[17]. The samples were air dried after exfoliation corrosion experiment.

Fig.1 Schematic diagrams of repair welding: (a) original welded joint; (b) groove machining; (c) repair welded joint

Fig.2 Sampling locations of the welded joint for exfoliation corrosion and electrochemical tests

Table 1 Chemical composition of two base alloys and filler metal (wt%)

Element	Zn	Mg	Cr	Cu	Ti	Mn	Zr	Fe	Si	V	Al
ER5356	0.10	4.50	0.15	0.10	0.14	0.10	-	-	-	-	Bal.
7N01-T5	4.48	1.55	0.23	0.11	0.05	0.29	0.18	0.13	0.05	0.01	Bal.
7N01-T4	4.76	1.20	0.11	0.01	0.04	0.42	0.07	0.11	0.04	0.01	Bal.

Table 2 Welding parameters of MIG welded joints

No.	Welding speed/mm·s⁻¹	Voltage/V	Current/A
1	8.5	27	290
2	8.5	27	290
3	7.5	27	290
4	6.5	28	290

Table 3　Abbreviations of specimens in Fig.2

Abbreviation	Meaning
AT4-BM	7N01 aluminum alloy under T4 condition
AT4-HAZ I	Location I of heat-affected zone of 7N01-T4 side
AT4-HAZ II	Location II of heat-affected zone of 7N01-T4 side
AT4	Location of all 7N01-T4 parts (AT4-BM+AT4-HAZ I+AT4-HAZ II)
WZ	Welded zone
AT5-HAZ I	Location I of heat-affected zone of 7N01-T5 side
AT5-HAZ II	Location II of heat affected zone of 7N01-T5 side
AT5-BM	7N01 aluminum alloy under T5 condition
AT5	Location of all 7N01-T5 parts (AT5-BM+A54-HAZ I+AT5-HAZ II)

In order to record the electrochemical behavior of specimens from different positions of repair welded joint (RWJ), the electrochemical tests were performed by CS350 electrochemical workstation. In the typical three-electrode system, the saturated calomel electrode (SCE) is the reference electrode, the platinum electrode is the auxiliary electrode and the studied alloy is working electrode. The size of the electrochemical test specimen is 15 mm×15 mm×5 mm, and the sampling location is displayed in Fig.2. The specimens were polished by SiC paper (roughness~2000#) gradually and then washed by alcohol. Additionally, the samples were dealt with ultrasonic cleaner before electrochemical testing. In order to stabilize the potential, the open circuit potential (OCP) experiment was conducted for 30 min, then dynamic potential polarization experiments for different positions of RWJ were conducted. The scanning speed is 1 mV·s^{-1} with the testing scope of −200~200 mV (relative to open circuit potential). Then the corresponding electrochemical parameters were obtained based on the polarization curves through Tafel-type fit of the data. The electrochemical impedance spectroscopy (EIS) tests were performed at OCP with the frequency range of 0.1 Hz~10 kHz. The electrochemical experiments were conducted in 3.5wt% sodium chloride solution at 25 °C with the exposed area of 1 cm^2.

2　Results

2.1　Microstructure analysis

For the age-strengthening aluminum alloys, the strength and corrosion susceptibility is mainly related to transformation of precipitates in different temperature ranges[15,18-20]. The distribution of precipitates in the original welded joint is shown in Fig.3[15] and the morphology of precipitates in different zones of RWJ is displayed in Fig.4. The distribution of precipitates in different locations of RWJ is mainly related to the initial state and thermal cycles during repair welding. On AT4 side, the non-continuous grain boundary precipitates form in the AT4-HAZ II (Fig.4a). The grain boundary precipitates in the AT4-HAZ I and AT5-HAZ I become more continuous compared to those in the original welded joint[15], which are harmful to the corrosion resistance of aluminum alloy, as displayed in Fig.4b and 4c, re-

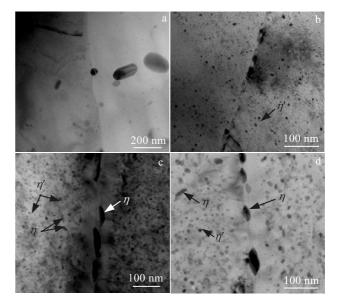spectively. Additionally, the volume of matrix precipitates increases in the AT5-HAZ II.

Fig.3　Precipitates in different areas of original welded joint: (a) AT4-HAZ II, (b) AT4-HAZ I, (c) AT5-HAZ I, and (d) AT5-HAZ II[15]
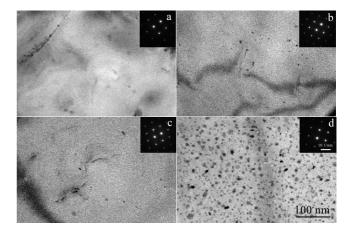

Fig.4　Precipitates in different areas of repair welded joint: (a) AT4-HAZ II, (b) AT4-HAZ I, (c) AT5-HAZ I, and (d) AT5-HAZ II

2.2 Corrosion properties

Fig.5 shows the evolution of exfoliation corrosion morphology of RWJ with different immersion time. A large number of bubbles appear at the initial stage of immersion corrosion experiment, which mainly occurs in the heat-affected zone. With the increase of immersion time, the exfoliation corrosion becomes severe and obviously occurs in the locations of HAZ I on both sides of RWJ after immersion for 2 h. The exfoliation corrosion grade on AT5-HAZ I and AT4 sides is defined as EA and EC, respectively. The exfoliation corrosion at AT5-HAZ I of RWJ is severer than that of the original welded joint after the same immersing time[15].

The IGC morphology of RWJ is displayed in Fig.6. It is obvious that the corrosion of AT4-HAZ I, covered by a large amount of white corrosion products, is the most serious, as shown in Fig.6a. Fig.6b shows the IGC characteristics of the original welded pass, and the white corrosion points are caused by the corrosion of phases around α-Al(Fe,Mn)Si in the matrix[21,22], which is common in aluminum alloys. The α-Al(Fe,Mn)Si phases fall off because of the corrosion of the surrounding matrix, and then a large number of corrosion pits form, as shown in Fig.6c. This phenomenon demonstrates that the corrosion of repair welded passes is more serious than that of the original ones. Additionally, the corrosion in AT4-HAZ I of RWJ is also more serious than that in the corresponding area of original welded joint[15], as displayed in Fig.6d and 6e.

2.3 Electrochemical test

In order to analyze the evolution of corrosion behavior of RWJ, the electrochemical experiments were conducted. Fig.7 displays the open circuit potential curves in different locations of RWJ. On AT4 side, the fluctuations of open circuit potential decrease and the open circuit potential moves towards the anode gradually with the increase of distance to the welded zone (WZ), while open circuit potential
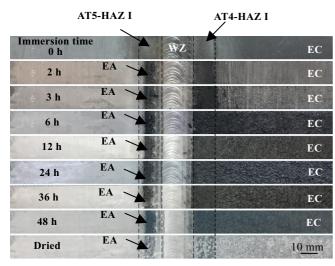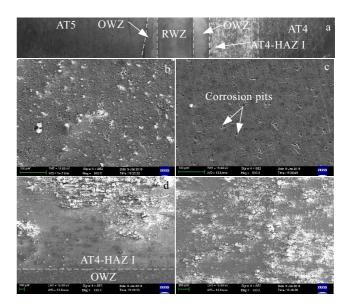

Fig.6 SEM images of repair welded joint after IGC for 6 h: (a) appearance of welded joint; (b) original welded zone (OWZ); (c) repair welded zone (RWZ); (d) transition area between original welded zone and AT4-HAZ I; (e) AT4-HAZ I

is still lower than that of WZ and AT5 side. Similarly, the open circuit potential moves to anode gradually with the increase of distance to WZ on AT5 side. The open circuit potential of AT5-BM is more positive than that of WZ. The difference of open circuit potentials in different locations of RWJ is probably associated with the transformations of microchemistry of grain boundary precipitates, which is mainly related to the welding thermal cycles and the initial state of Al-Zn-Mg(Cu) alloys[15,19,20].

The cathodic polarization curves in different zones of RWJ are similar, while the anodic polarization curves in different locations of RWJ display different characteristics, as shown in Fig.8. As the over-potential of the anode increases, the polarization current density on the AT4 side rapidly increases and then gradually approaches a certain stable value. The change of anodic polarization curves on AT5 side can be divided into three stages: first, slow increase; second, fast-rising stage; finally, certain stable value. The main reasons for the difference of polarization curves are related to the difference of element contents, morphology and volume of precipitates in different locations of RWJ.

Generally speaking, the corrosion susceptibility of 7N01 aluminum alloys can be evaluated by the electrochemical parameters obtained from the polarization curves, such as corrosion current density (i_{corr}) and corrosion potential (E_{corr}). The parameters in Table 4 illustrate that the difference of corrosion current density on AT5 side is not obvious.

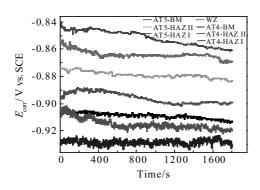Fig.5 Evolution of exfoliation corrosion for repair welded joint

Fig.7   Evolution of open circuit potential in different locations of repair welded joint for different immersion time
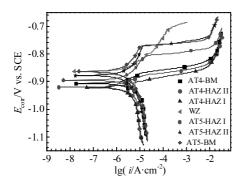

Fig.8   Dynamic potential polarization curves in different areas of repair welded joint

On AT4 side, the corrosion current density of AT4-BM is the lowest with the value of $2.5×10^{-7}$ A·cm^{-2} and the corrosion current density of WZ is $6.7×10^{-7}$ A·cm^{-2}. The greater

the corrosion current density, the larger the corrosion rate, which reflects poor corrosion resistance of the alloy. However, the evolution of corrosion susceptibility in different positions of RWJ cannot be evaluated through the corrosion current density based on the results of immersion corrosion test. The reason is that the polarization experiments should be conducted by exposing different locations of RWJ independently and the relevant electrochemical parameters should be obtained under uncoupled situation, while all the zones in actual welded joint are galvanically coupled.

Fig.9 shows the characteristic of EIS results with Nyquist and Bode-phase data. In high-frequency area, the Nyquist impedance diagrams consist of a capacitive reactance arc, and a line with tilt angle appears in the low-frequency location, which indicates the occurrence of diffusion procedure, namely Warburg impedance[23,24]. All the maxima of phase angle in Bode plots are lower than 90°, which represent the appearance of a deviation of ideal-capacitance on the electrochemical interface, as shown in Fig.9b. The equivalent circuit was obtained through Zsimpwin software to analyze the corresponding electrochemical data. R_{ct} means the charge transfer, R_s is the solution resistance and W represents the Warburg impedance, as shown in Fig.10. In real electrochemical behavior, there is no pure capacitance. Consequently, the constant phase element (CPE) is widely used in the equivalent circuit to get more accurate fitting results. The corresponding electrochemical parameters are listed in Table 5. The location of AT4-BM has the maximum charge transfer impedance with the value of 5.54 kΩ·cm^2, while the charge transfer impedance of AT5-BM is the lowest. The higher R_{ct} value means lower corrosion current density, so the alloy has better corrosion resistance.

Table 4   Electrochemical parameters in different areas of RWJ in 3.5wt% NaCl solution

Specimen	E_{corr}/mV vs. SCE	i_{corr}/×10^{-6} A·cm^{-2}	β_a/mV·dec^{-1}	B_c/mV·dec^{-1}
AT5-BM	−863±8	3.9±0.2	189±4	163±6
AT5-HAZ II	−878±3	3.3±0.4	130±5	168±7
AT5-HAZ I	−895±2	2.4±0.2	88±4	92±5
WZ	−863±4	0.67±0.03	32±6	67±4
AT4-HAZ I	−921±3	1.1±0.2	20±3	74±4
AT4-HAZ II	−924±2	1.2±0.3	45±6	52±5
AT4-BM	−906±3	0.25±0.02	17±3	42±4

3   Discussion

During the nucleation and growth of precipitates in Al-Zn-Mg(Cu) alloy, GP zone forms during 20~120 °C, η' phase forms from 120 °C to 250 °C, and η phase forms during 150~300 °C [7]. Meanwhile, the corresponding dissolution temperature ranges of precipitates in Al-Zn-Mg(Cu) alloys are: 50~150 °C for GP zones, 200~250 °C for η' pre-

cipitate, and 300~350 °C for η precipitate[25]. The maximum temperature reduces with the increase of the distance to fusion line during welding process and the temperature range of HAZ I and HAZ II of welded joint is 300~400 °C and 150~300 °C, respectively, according to the Rosenthal's model[15]. Then the main variation of HAZ I adjacent to WZ is the dissolution of precipitates and the diffusion of solute

elements from the matrix to grain boundaries, according to the temperature range of the formation and dissolution of the precipitates in Al-Zn-Mg(Cu) alloy. The repair welding process further causes the segregation of solute element Zn, which exists as two forms: (I) stable grain boundary precipitates; (II) solute element.

The results of immersion corrosion tests prove that the difference of corrosion susceptibility of RWJ is evident. The difference of corrosion potential in various positions of RWJ induces the galvanic corrosion in corrosion medium. The AT4 side of RWJ has the highest corrosion susceptibility during galvanic coupling due to the lowest corrosion potential. Additionally, the galvanic corrosion between different locations is associated with the distance between them, because the cathodic polarization behavior is mainly dominated by diffusion course[13]. Accordingly, the corrosion in AT4-HAZ I and AT5-HAZ I is severer than that in base metals. The evolution of corrosion susceptibility of

RWJ in this research is similar of that in Peng's research[1]. Actually, the root cause of the variation of the corrosion susceptibility of RWJ is associated with the content of aluminum alloy elements[20,26]. The relevant researches demonstrated that the potential of Zn is lower than that of aluminum matrix, while the potential of Cu is positive to aluminum matrix[27,28]. Consequently, the difference of corrosion potential in different locations of RWJ is caused by the variance of Zn and Cu contents, as displayed in Table 1 and Table 4.

Additionally, the repair welding deteriorates the corrosion resistance of HAZ I. The main reason is likely associated with the transformation of precipitates and diffusion of alloy elements, especially the Zn and Cu elements, caused by the extra thermal cycles. For the HAZ I, the transformation refers to the dissolution of matrix precipitates and the diffusion of solute elements from the aluminum alloy matrix to grain boundaries (Fig.4). Since the corrosion of
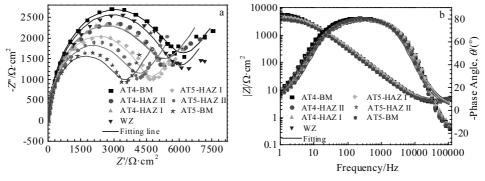

Fig.9 Impedance spectra in different locations of repair welded joint: (a) Nyquist plots and (b) Bode plots
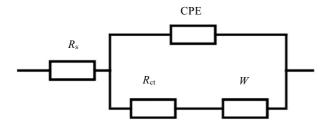

Fig.10 Equivalent circuit

aluminum alloy is caused by the corrosion potential difference between the grain boundaries and aluminum matrix[20], the electrochemical potential of grain boundaries and aluminum alloy matrix should be considered. The increase of Zn reduces the electrochemical potential[20]. The influence of Cu content on the electrochemical potential can be neglected considering the content is low, as listed in Table 1. Consequently, the variation of electrochemical potential is mainly caused by the change of Zn content. For the aluminum matrix, the dissolution of precipitates leads to the re-

Table 5   Electrochemical parameters obtained from equivalent circuit diagram

Specimen	$R_s/\Omega\cdot cm^2$	CPE		$R_{ct}/k\Omega\cdot cm^2$	$Y_w/\times 10^{-5}\ \Omega\cdot cm^2\cdot s^{0.5}$
		$Y_0/\times 10^{-6}\ \Omega\cdot cm^2\cdot s^n$	$n\ (0<n<1)$		
AT5-BM	4.33	7.22±0.52	0.96	3.13±0.14	5.34±0.71
AT5-HAZ II	4.24	7.44±0.47	0.94	3.73±0.16	5.18±0.70
AT5-HAZ I	4.30	6.52±0.43	0.94	4.28±0.18	6.03±1.10
WZ	4.33	7.07±0.44	0.93	5.47±0.24	5.75±1.22
AT4-HAZ I	4.45	8.02±0.41	0.92	5.13±0.18	6.89±0.13
AT4-HAZ II	4.30	7.11±0.47	0.93	4.79±0.24	4.29±0.77
AT4-BM	4.22	7.16±0.45	0.94	5.54±0.26	4.43±0.80

duction of electrochemical potential[19], and the electrochemical potential of grain boundaries also becomes more negative due to the diffusion of Zn. It is reasonable to speculate that the negative influence of Zn diffusion from the matrix to grain boundaries exceeds the positive influence of the dissolution of matrix precipitates, so the corrosion potential difference between the matrix and grain boundaries increases. Therefore, the corrosion susceptibility of HAZ I increases after repair welding. The similar phenomenon is proved in the relevant literatures[19,20].

4 Conclusions

1) Galvanic corrosion forms due to the corrosion potential differences at different locations of repair-welded joint. The 7N01-T4 aluminum alloy side displays the lowest corrosion resistance owing to the lower corrosion potential during galvanic corrosion.

2) The repair welding deteriorates the corrosion resistance of heat-affected zone because the transformation of precipitates and diffusion of Zn from the matrix to grain boundaries caused by extra thermal cycles increase the corrosion potential difference between the matrix and grain boundaries.

References

1 Peng X Y, Cao X W, Xu G F *et al. Journal of Materials Engineering and Performance*[J], 2016, 25(3): 1028
2 Liu D M, Xiong B Q, Bian F *et al. Materials & Design*[J], 2014, 56: 1020
3 Huang L P, Chen K H, Li S. *Materials Science and Engineering B*[J], 2012, 177(11): 862
4 Wang X M, Li B, Li M X *et al. Materials Science and Engineering A*[J], 2017, 688: 114
5 Zhang F, Su X K, Chen Z Y *et al. Materials & Design*[J], 2015, 67: 483
6 Yan S H, Chen H, Ma C P *et al. Materials & Design*[J], 2015, 88: 1353
7 Deng Y, Ye R, Xu G F *et al. Corrosion Science*[J], 2015, 90: 359
8 Qiao J N, Lu J X, Wu S K *et al. International Journal of Fatigue*[J], 2017, 98: 32
9 Marlaud T, Malki B, Henon C *et al. Corrosion Science*[J], 2011, 53(10): 3139
10 Liu B, Zhang X X, Zhou X R *et al. Corrosion Science*[J], 2017, 126: 265
11 Couturier L, Deschamps A, De Geuser F *et al. Scripta Materialia*[J], 2017, 136: 120
12 Maya-Johnson S, Santa J F, Mejía O L *et al. Metallurgical and Materials Transactions B*[J], 2015, 46(5): 2332
13 Venugopal A, Sreekumar K, Raja V S *et al. Metallurgical and Materials Transactions A*[J], 2010, 41(12): 3151
14 Wang X D, Mao S C, Chen P *et al. Materials & Design*[J], 2016, 90: 230
15 Li S, Dong H G, Shi L *et al. Corrosion Science*[J], 2017, 123: 243
16 GB/T22639-2008[S], 2008 (in Chinese)
17 GB/T 7998-2005[S], 2005 (in Chinese)
18 Li S, Guo D, Dong H G *et al. Transactions of Nonferrous Metals Society of China*[J], 2017, 27(2): 250
19 Li S, Dong H G, Li P *et al. Corrosion Science*[J], 2018, 131: 278
20 Song F X, Zhang X M, Liu S D *et al. Corrosion Science*[J], 2014, 78: 276
21 Allachi H, Chaouket F, Draoui K *et al. Journal of Alloys and Compounds*[J], 2010, 491(1-2): 223
22 Szklarska-Smialowska Z. *Corrosion Science*[J], 1999, 41(9): 1743
23 Macdonald D D. *Electrochimica Acta*[J], 2006, 51(8-9): 1376
24 Feng X G, Lu X Y, Zuo Y *et al. Corrosion Science*[J], 2016, 103: 223
25 Nicolas M, Deschamps A. *Acta Materialia*[J], 2003, 51(20): 6077
26 Liu S D, Li C B, Deng Y L *et al. Materials Chemistry & Physics*[J], 2015, 167: 320
27 Liu S D, Chen B, Li C B *et al. Corrosion Science*[J], 2015, 91: 203
28 Wloka J, Hack T, Virtanen S. *Corrosion Science*[J], 2007, 49(3): 1437

补焊对 7N01 合金焊接接头腐蚀行为的影响

李 帅 [1,2]，刘中英 [1]，王星星 [1]，毛 丰 [2]，夏月庆 [1]，纠永涛 [3]，上官林建 [1]，龙伟民 [3]
(1. 华北水利水电大学 机械学院，河南 郑州 450045)
(2. 河南科技大学 金属材料磨损控制与成型技术国家地方联合工程研究中心，河南 洛阳 471003)
(3. 郑州机械研究所 新型钎焊材料与技术国家重点实验室，河南 郑州 450001)

摘 要：实际生产过程中，补焊过程往往对焊接接头的可靠性产生影响。研究了补焊对 7N01-T5/7N01-T4 异种铝合金腐蚀性能的影响。结果表明，补焊会导致焊接接头耐蚀性降低，特别是热影响区域。焊接接头腐蚀性能演变主要与补焊过程中 Zn 元素从基体向晶界处的扩散有关。
关键词：MIG焊；补焊；7N01铝合金；腐蚀行为；热影响区；热循环

作者简介：李 帅，男，1986 年生，博士，讲师，华北水利水电大学机械学院，河南 郑州 450045，电话：0371-69127295，E-mail: lyctlishuai@163.com